Tribology in Industry

Investigation of Microstructural Characterization and Mechanical Properties of 8YSZ Thermal Barrier Coatings: Atmospheric Plasma Spray versus Electron Beam-Physical Vapour Deposition

Prajakta Nikhil Kadam[a,b], Dattataraya Bhise[b], Nikhil Rajendra Kadam[b,*], Vijay Kolate[c], Khandu Gavali[c], Satish Deshmukh[d]

[a]Department of Mechanical Engineering, JSPM's Group of Institutes, BSIOTR, Pune, Maharashtra, India 412 207,
[b]Department of Mechanical and Manufacturing Science, JSPM University, Pune, Maharashtra, India 412 207,
[c]Department of Mechanical Engineering, Trinity Academy of Engineering, Pune, Maharashtra, India 411 048,
[d]Department of Civil Engineering, Trinity Academy of Engineering, Pune, Maharashtra, India 411 048.

A B S T R A C T

In this study, the formation and growth of coating microstructure was studied and reported based on APS and EB-PVD deposition mechanism with the change in spray angle. A NiCrAlY bond coat with 8YSZ ceramic coat was applied by APS and EB-PVD deposition onto the Inconel 718 with the variation in spray angle. The investigation was divided into microstructural analysis and mechanical properties to determine the effect of different deposition mechanism and its variation in spray angle. The results obtained show that the APS with 60° spray angle has more presence of defects, followed by APS 90° and EB-PVD samples. The APS avg. grain size varies between- 400 to 800nm, whereas EB-PVD in between- 150 to 300nm. The EB-PVD with 90° spray angle results in low porosity i.e. 18.12 % followed by APS 90°, EB-PVD 60°, and APS 60° spray angle, respectively. The low porosity results in high compressive residual stress than medium and high porosity. The avg. Raman shift for EB-PVD 90° spray angle i.e. low porosity is 1.86 cm^{-1}, for medium i.e. APS 90° and EB-PVD 60° is 1.33cm^{-1} and 1.53cm^{-1} respectively, and for high porosity is 0.93cm^{-1}. The 90° spray angle showed better microstructural and mechanical properties compared to 60°.

1. INTRODUCTION

Thermal barrier coatings (TBCs) are functional ceramic coatings widely applied onto the gas turbines and aero engines. The role of successful applications of these ceramic coatings onto the hot components made up of nickel based superalloy is to protect against oxidation and erosion [1–3]. With applications of TBCs which possesses low thermal conductivity and high coefficient of thermal expansion (CTE) leads to increase in durability, performance and efficiency with rise in

temperature capabilities [3]. The TBCs applied onto the superalloy reduces fatigue due to thermal and creep with the reduction of temperature and driving force providing thermal barrier against corrosion and oxidation [1, 4]. The metallic bond coat provides adhesion property to superalloy substrate for application of ceramic top coat [1, 5]. In addition, it also reduces CTE mismatch between substrate and ceramic top coat [4-5]. Typically 7-8 wt. % yttria stabilized zirconia (YSZ) is used as the most important candidate material as it shows low thermal conductivity and high coefficient of thermal expansion. Generally, the major ceramic coatings used on gas turbines and aero engines are applied using Atmospheric Plasma Spray (APS) and Electron Beam Physical Vapour Deposition (EB-PVD) mechanism. The TBCs are exposed to high temperature severe environments with working at non-uniform in pressure, oxidizing, corrosion conditions [1]. Theses working conditions can lead to early damage in TBCs and can grow with time resulting in failure of the system. There are many factors which influences the durability of the TBCs such as microstructural defects like cracks & pores, and mechanical properties. These are dependable on deposition mechanism and its spraying parameters along with the use of different ceramic materials for top coat [1, 3]. Hence, this develops the need of understanding the effect and contribution of deposition mechanism, behaviour of different ceramic materials along with the working environment to develop durable TBCs [1, 3-4].

Ling et al. [6] found the effect of spray distance on coating structure producing dense grains leading to improve hardness. Also, Dipak [7] and Mantry et al. [8] investigated the effect of spray conditions contributing to change in roughness and thickness of the structure. John et al. [9] and Morks et al. [10] added rare earth elements with surface re-melting and glazing operation to improve the hardness and can control the level of porosity. Izadinia et al. [11] also contributed to improve hardness and reduction in porosity with variation in spray conditions to obtain conventional splats with segmented cracks. In addition to spray parameters, Wang et al. [12], Zhu and Ma [13], and Ekberg et al. [14] also investigated the effect of feedstock and heat treatment which would affect the properties and coating structure. Even the effect of spray angle impacted on the formation and behaviour of grain growth structure which was found by Schulz et al. [15-16]. Zang et al. [17] and Ganvir et al. [18] reduced the thermal

conductivity with formation of porous coating structure with change in spray parameters. Powell et al. [19] found the effect of structured and elevated porosity which affects the grain growth leading to produce more rough surface texture in case of elevated porosity formation. Cui et al. [20] found the presence of more radial crack formation in high porous region whereas more axial cracks in low porous region resulting in penetration of cracks towards bond coat from top coat. Jang and Matsubara [21] found the indirect relationship of hardness and young's modulus with respect to porosity. Also, Krishnasamy et al. [22] found the effect of porous structure on fracture of coating to predict the crack length which results decrease in coating integrity with increase in pores size. In addition to spray parameters, Zhang et al. [23] found the effect of change in temperature and velocity of in-flight particles showing better melting resulting in fully melted particles travelling towards substrate. These leads to generation of better coating structure in terms of few defects compared to partially melted particles. Myoung et al. [24] studied the use of multiple hopper system to control the change in feedstock rate for formation of dense coating microstructure. Even the feedstock powder shape and size affects the bonding strength and addition to porous structure which was found by Shi et al. [25]. Kadam et al. [26-27] investigated and found the effect of spray parameters resulting on to the change in coating hardness and roughness leading to improve the performance of the system. Teixeira et al. [28] found the effect of rise in substrate temperature resulting in the generation and change of residual stresses from tensile to compressive during thermal loading. Scrivani et al. [29] and Portinha et al. [30] investigated the effect of porosity on residual stresses and found that the compressive residual stresses increases after annealing followed by thermal stock. From above survey, it was found that the spraying parameters plays an important role in formation of coating structure and properties of the TBCs, this study can provide a better understanding of the TBCs.

In this study, the formation and growth of coating microstructure was studied and reported based on APS and EB-PVD deposition mechanism with the change in spray angle. A NiCrAlY bond coat with 8YSZ ceramic coat was applied by APS and EB-PVD deposition onto the Inconel 718 with the variation in spray angle. The investigation was divided into microstructural analysis and mechanical

properties to determine the effect of different deposition mechanism and its variation in spray angle. These studies reveal a change in formation and growth of coating structure and its properties indicating unique grain growth structure with presence of few defects like cracks and pores. It was also used to discuss the coating mechanism to provide the strong support for the research and development of TBCs with different deposition mechanism and variation of spraying parameter.

2. EXPERIMENTATION

2.1 Preparation of APS/EB-PVD 8YSZ coatings

A NiCrAlY (AMDRY 962) bond coating was sprayed on Inconel 718 using APS. The APS substrate was a square shaped Nickel based superalloy with dimensions of 20mm and 3mm in thickness. The substrate surface before and after bond coating was polished and grit blasted with alumina powder to improve the surface roughness, thus increases bond strength with 8YSZ ceramic top coating [27,31]. The 8YSZ (powder provided by Oerlikon Metco, 204B-NS) was deposited as top coat onto the bond coat using APS and EB-PVD deposition mechanism with variation of spray angle. The bonding coat thickness was sanded to 90-100 μm and top coating was deposited approx. to 300±25 μm.

In both deposition mechanism, the change in spray angle is denoted by normal (90°) and inclined (60°) spray angle respectively. As thumb rule, the normal spray angle is perpendicular to the substrate to be coated i.e. line of sight. The deviation from normal spraying angle can compromise the coating properties. The low velocity process needs to stay within ±15° of normal and high velocity process can tolerate off-axis spray up to ±45° [32]. The reason behind selection of 60° angle is to avoid the wastage of coating feedstock, as the lower spray angle could lead to more elongation in the coating structure with large amount of wastage in the material [33-34]. Fig. 1 shows the schematic diagram of spray angle direction with respect to substrate surface used in APS and EB-PVD deposition process. In APS process, the substrate is fixed and the plasma gun is inclined as per the required spray angle, whereas in EB-PVD process, the electron beam inclination is fixed, i.e., 270° and the mounting of substrate is change as per the spray angle requirement.
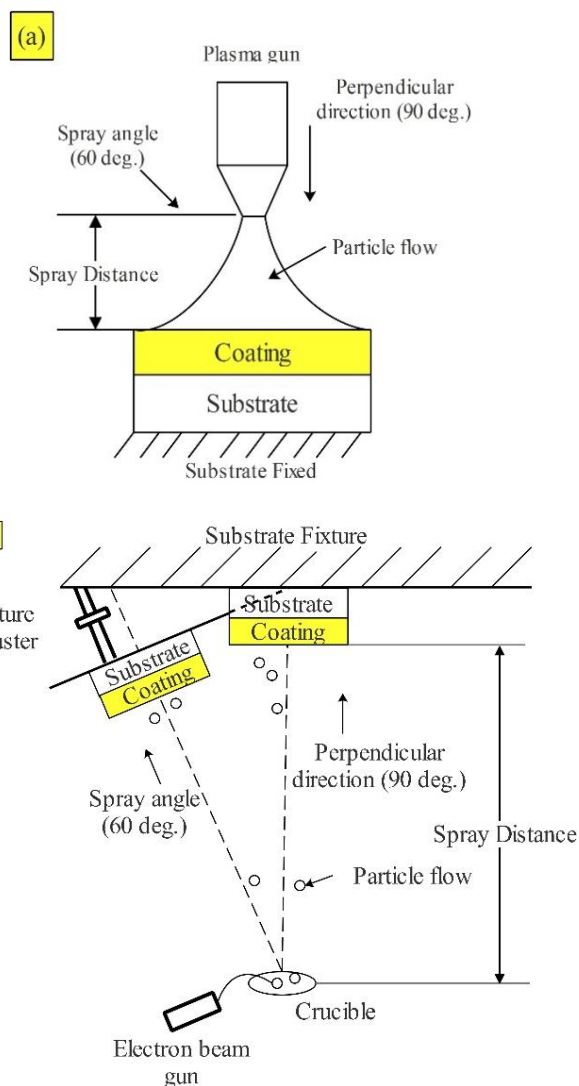

Fig. 1. Schematic showing variation of spray angle direction for (a) APS and (b) EB-PVD.

In present work, the bond coat for all samples were deposited in one pass with similar spraying parameters using APS to reduce variation in structure. A few top coat samples were deposited by APS and few with EB-PVD to compare with variation of spray angle. Figure 2 shows the thermal spray and electron beam facility used to produce coatings. The thermal facility was available at Spraymet Surface Technologies Pvt. Ltd., Bangalore and EB-PVD with BITS Pilani, K. K. Birla Goa Campus, Goa. The detailed spraying parameters is listed in Table 1. Figure 3 shows the 8YSZ TBC samples deposited by APS and EB-PVD process with the change in spray angle 90° and 60°. The notations used for APS deposited samples were A90 and A60 and EB-PVD were called by E90 and E60 for spray angle of 90° and 60° respectively.

Table 1. Detailed spray parameters [23,27].

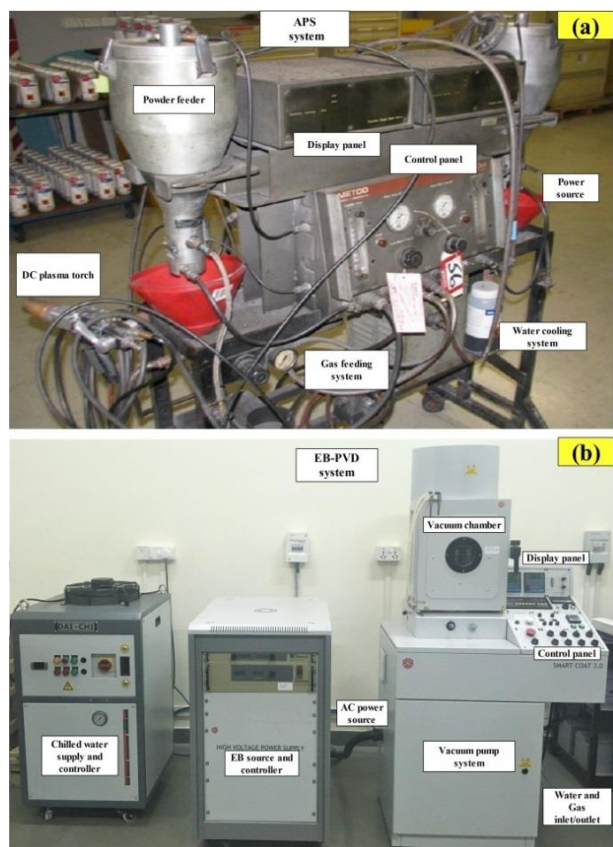| Process parameters	Bond coat	Top coat	
Deposition process	APS	APS	EB-PVD
Feedstock powder	NiCrAlY	8YSZ	
Current (A)	400	500	24
Filament current (mA)	-	-	40
Voltage (KV)	60	65	5.8
Spray distance (mm)	90	90	90
Spray Angle (°)	90	60 and 90	

Fig. 2. (a) APS (Make: Sulzer Metco AG, Switzerland) and (b) EB-PVD (Make: High Hind Vacuum Ltd., Bangalore) [26].
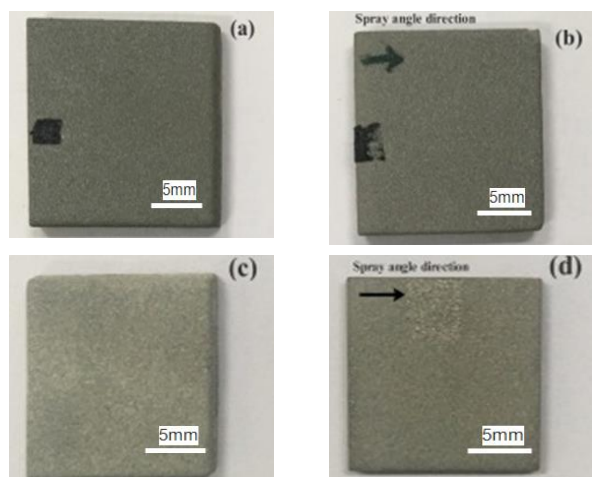

Fig. 3. Plasma sprayed with (a) 90° and (b) 60° [35], EB-PVD sprayed with (c) 90° and (d) 60° spray angle [23].

2.2 Analysis methods

The microstructures were characterized using scanning electron microscopy (SEM; Make: Quanta FEG 250, Hillsboro, USA). Additionally, the presence of porosity was calculated by ImageJ software using high magnified microstructure images [36–38].

Raman Spectroscopy (Make: Lab Ram spectrometer, HORIBA Jobin Yvon, France) was used to calculate the generation of residual stress during thermal loading. The relative amount of various phases was measured using argon-ion laser of wavelength λ=532nm with power of 5mW. The coating specimen were heated upto the temperature of 500°C, followed by dwell and cooling cycle each for the duration of 10mins.

The indentation test was performed to analyze the hardness (HV) using quad pyramid diamond indenter (Make: Matsuzawa VMT-7). Each indentation performed used a maximum load of 5kgf with the hold time of 10sec. The surface generated were measured using surf test profilometer (Make: Mitutoyo SJ 410, Japan) to obtained the arithmetic mean surface roughness.

3. RESULTS AND DISCUSSION

3.1 Surface morphology of 8YSZ TBCs

The microstructures of 8YSZ TBCs produced with APS and EB-PVD deposition mechanism with variation of spray angle is shown in Figure 4 and Figure 5. The APS enabled 8YSZ samples are noted as A90 and A60, whereas the samples deposited by EB-PVD are noted by E90 and E60. During APS and EB-PVD deposition, the molten particles are bombarded on the substrate and quickly solidifies forming coating. The duration is too short (about 20 sec.) that the first particles has solidifies to layer before the second particles bombards on the surface. The time from melted particles bombards to solidified layer is too short (about 20 sec.) that the molten particle does not cover the entire previous layer leading to the formation of cracks. These molten particles create the high flattering and smooth surface with presence of few defects such as cracks and pores in the coating. Whereas, few partially melted results in low

flattering leading to high porous structure. This leads to generation of rough surface creating poor adhesion between deposited and

upcoming layer. The spray angle plays an important role in generation and formation of different grain size, pores and cracks [39].
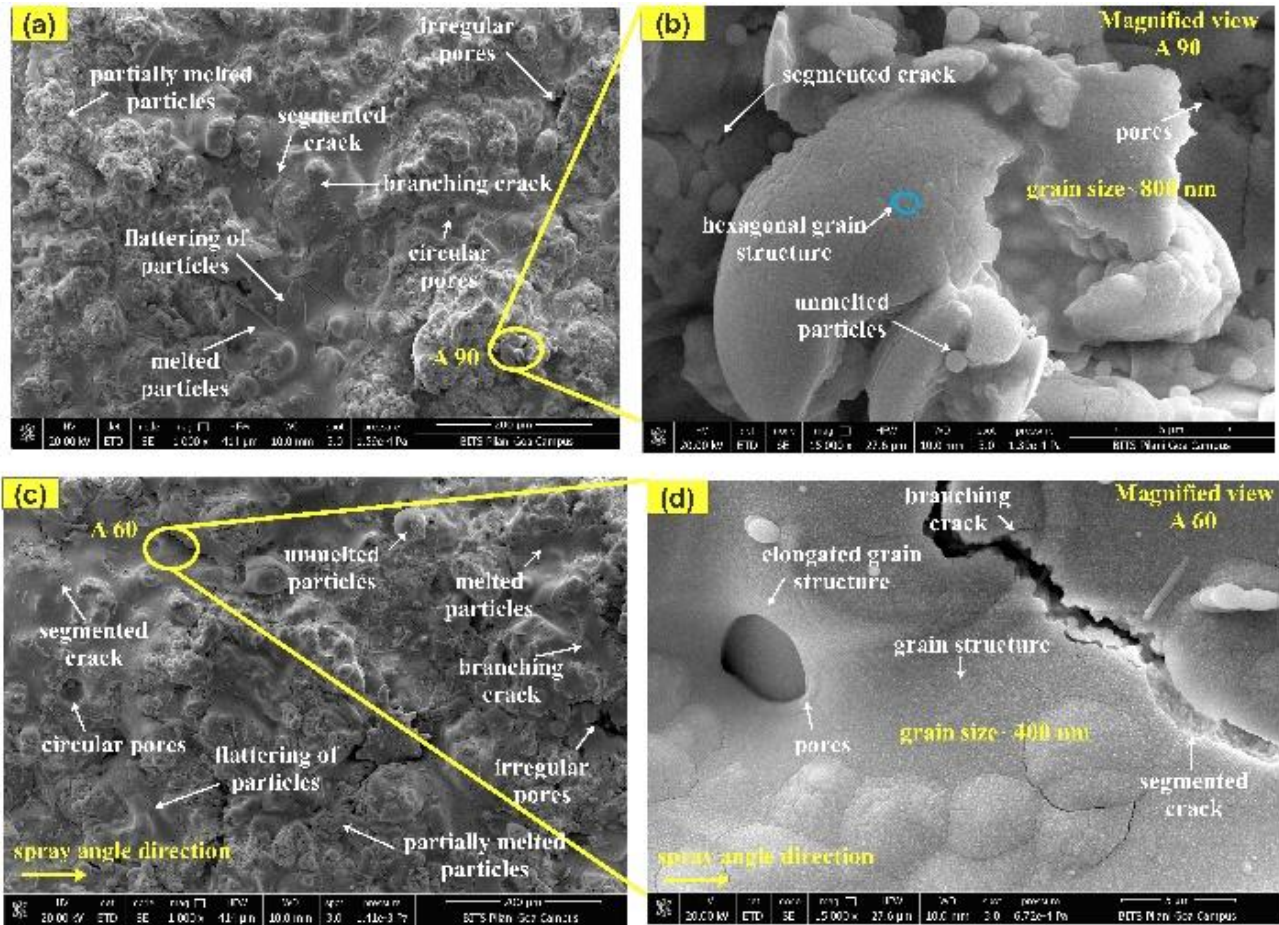

Fig. 4. APS Microstructure with changed spray angle of (a) 90°, (b) magnified 90°, (c) 60° and (d) magnified 60° [35].

Figure 4 (a) and (c) shows the APS deposited 8YSZ TBC with spray angle of 90° and 60°. In APS deposition, A90 sample shows the uniform surface with high flattering compared to A60 sample. Also, the structure with A60 shows the presence of more defects like cracks and pores. The crack propagation leads to formation of segmented and branching cracks. Due to presence of more crack generation, the coating may result to early failure compared to A90 sample. The presence of segmented cracks at certain level improves the strain tolerance and provides high young's modulus to coating [40-41]. The horizontal crack growth causes the crack to penetrate resulting in vertical crack generation. The generation and formation of horizontal and vertical cracks were observed in both spray angle deposition mechanism. The horizontal crack runs through dense region contributing to less spallation compared to vertical crack as it can separate the splat layer structure contributing to premature

and early failure due to spallation. Figure 4 (b) and (d) shows the higher magnification view of A90 and A60. The rapid solidification of melted particles leads in crack formation. The A60 sample shows high presence of cracks and pores compared to A90 with more width causing in generation of high thermal stresses. The A90 shows a small opening of segmented crack showing low significance to the formation of branching cracks. The hexagonal grains with boundaries and inter-crystalline space were visible with spray angle. Only the change in grain size and shape was observed with changed spray angle. In A90, the grain boundary with equiaxed size is observed with small elongation in the grains. Whereas, in A60, the grain boundary with large amount of elongation was observed. A similar study was reported by Montavon et al. [33] and Kadam et al. [40] which showed splat elongation was affected with change in spray angle. The more presence of defects leads to fast cooling which

affects the formation of grains leading to brittle failure. The A90 and A60 shows the avg. diameter of grain structure of ∼ 800 nm and 400 nm respectively. It means that the A90 grain is around double in size compared to A60 resulting in low shadow region.

Figure 5 (a) and (c) shows the EB-PVD deposited 8YSZ TBC with spray angle of 90° and 60°. The E90 shows the uniform surface with high flattering compared to E60. Also, the structure with E60 shows more presence of defects in the coating. Figure 5 (b) and (d) shows the higher magnification view of E90 and E60. The effect of spray angle results change in grain structure and dissimilar grain growth. The E90 sample shows hexagonal grain with avg. grain size of ∼ 150 nm and E60 shows elongated grain with avg. grain size of ∼ 300 nm. The E90 showed dense grain structure with few defects whereas the E60 showed distributed grain structure with more defects present resulting in more shadow region.
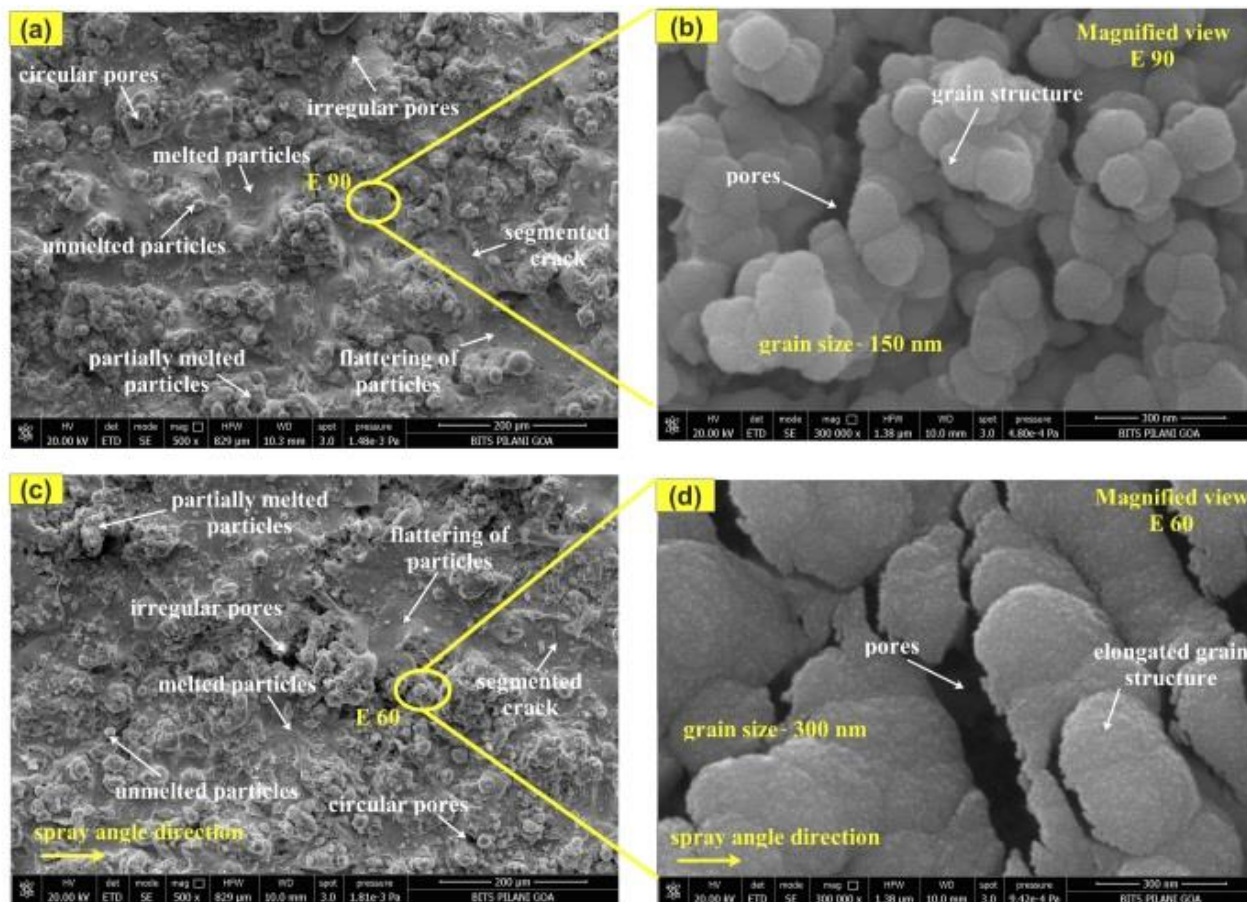

Fig. 5. EB-PVD Microstructure with changed spray angle of (a) 90°, (b) magnified 90°, (c) 60° and (d) magnified 60° [27].

In current work, the spray angle considered was 90° and 60° for APS and EB-PVD deposition mechanism. The spray angle affects the coating structure in terms of grain growth behavior, presence of defects such as pores, cracks and surface irregularities, and mechanical properties. In case of normal spray angle (90°), the coating is evenly distributed onto the substrate whereas in 60°, the substrate surface is tilted with respect to normal axis which results change in small spray distance between both ends of substrate developing tapered coating pattern (Refer Figure 1). Due to this, one end is closer to the spray gun compared to the opposite end which results flow of

molten particle in inclined direction. This could lead in uneven coating surface produced resulting change in coating microstructure. The low particle velocity and peening at longer side showed generation of low compressive residual stresses. In 90°, the spray coverage is small whereas 60° refers to large coverage area resulting in spray spot elongation in the direction of spray angle. The decrease in spray angle leads to generate a broader spray spot in the direction of spray gun tilt. A similar feature was observed by Montavon et al. [33], with a decrease in spray angle leading to generating a broader spot. The 60° spray angle distributes droplets to more space which results

less recombination leading to high atomization, whereas 90° will distribute more evenly due to less spread out chances and forms high concentration spot. These phenomenon develops porosity affecting the hardness and roughness. The increase in porous structure results in more surface irregularities, which cause a decrease in hardness [17-20]. Based on the literature, it can be relatable that the increase in porous structure in the coating would lead to a decrease in hardness and an increase in surface irregularities. In APS, the molten particles are in large size compared to EB-PVD process, as it uses plasma source to heat and melt the feedstock whereas, the electron beam is used in EB-PVD to melt the particles. The 90° spray angle results in more deposition onto the vertical substrate which can reduce the porous structure resulting in low shadow region. The more porous structure showing high shadow region results in lower value of coating hardness and poor surface finish. Kadam et al. [27] also found a similar coating structure with varying spray angle parameters, resulting in more porosity and a high shadow region. The EB-PVD coated E90 and E60 samples show more uniform surface with fine and dense grain growth compared to APS enabled A90 and A60 samples. Also, the presence of defects in E90 and E60 were less compared to A90 and A60. The more amounts of horizontal cracks were visible in APS deposited coating which could result in early failure to spallation. Also, Kadam et al. [42] found that horizontal and vertical cracks were generated during coating deposition with the plasma spray process. The high flattering was observed in E90 and E60 with uniform grain distribution. The EB-PVD process showed the smaller grain structure in terms of size and shape compared to APS process which results in dense grain growth behavior. The EB-PVD results in low shadow region contributing to low porosity compared to large shadow region observed in A90 and A60.

3.2 Cross-sectional morphology of 8YSZ TBCs

Figure 6 shows the comparison of cross-sectional structure of APS deposited TBCs with two different spray angle.
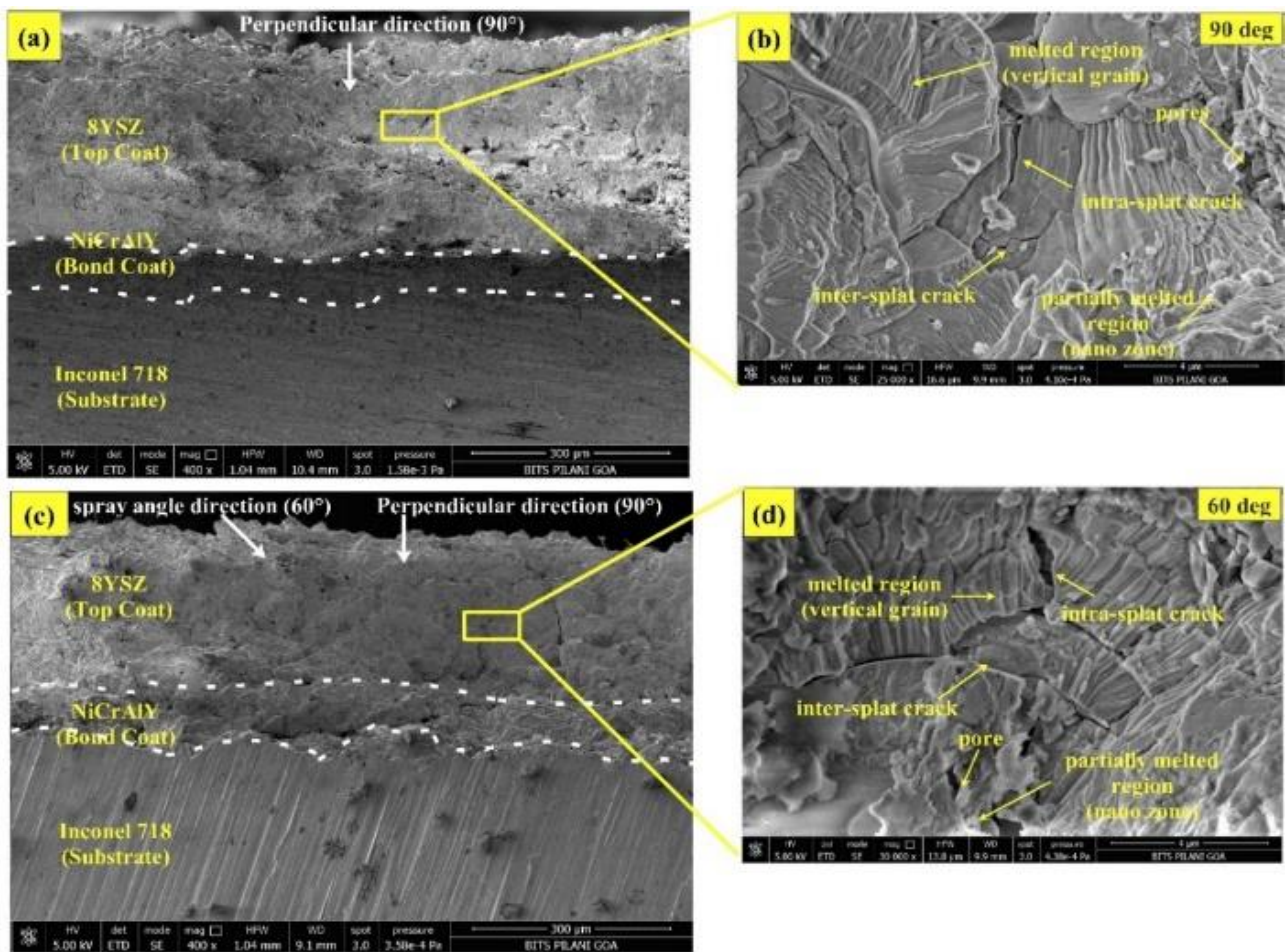

Fig. 6. APS Cross-sectional microstructure with changed spray angle of (a) 90°, (b) magnified 90°, (c) 60° and (d) magnified 60° [43].

All three layers of TBC system are identified namely Inconel 718 substrate, NiCrAlY bond coat, and 8YSZ topcoat. Both the cross-section consists of melted and partially melted region with few defects such as pores, inter-crack and intra-cracks. The topcoat showed the individual splats which can be clearly identified revealing the unique characteristics of APS process. Most of the splat present in the coating is visible as the single splats. The continuous deposition of molten particles leads to overlapped splats creating the multiple coating layers. In 90° spray angle, the splats are parallel to the substrate surface whereas the 60° angle showed parallel splats with few inclined to substrate. In inclined spray angle, the width and length of splats were more with splats inclination towards the spray angle direction. The vertical grain growth shows the strong bond over two splats. Both spray angle showed inter-splats and intra-splats

cracks formed in the splat layer structure. During deposition, the lack of complete overlap of adjacent splat and gas entrapment results in the generation of inter-splat crack. Whereas the intra-splat cracks are formed due to shrinkage and solidification of splats.

Figure 7 shows the comparison of cross-sectional structure of EB-PVD deposited top coat TBC with two different spray angle. All three layers of TBC system are identified namely Inconel 718 substrate, NiCrAlY bond coat, and 8YSZ topcoat. Both the spray angle condition showed the presence of fully melted and partially melted particles with defects such as pores and voids. From figure 7, it is clear that the EB-PVD top coat thickness is small compared to APS process. Therefore, the high magnification images were captured on the topmost part of the coating structure.
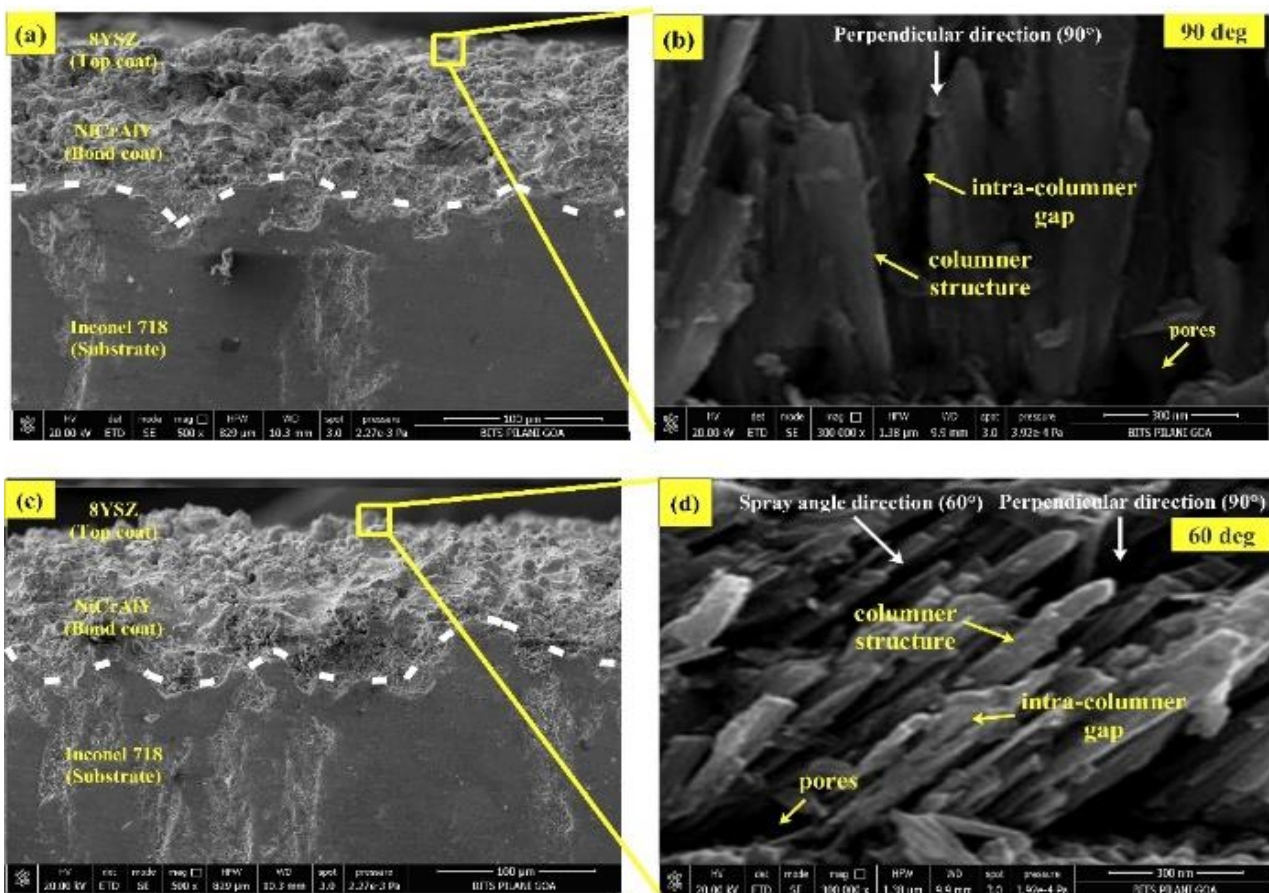

Fig. 7. EB-PVD Cross-sectional microstructure with changed spray angle of (a) 90°, (b) magnified 90°, (c) 60° and (d) magnified 60° [43].

The coating structure showed the individual columns which clearly identifies the unique characteristics of EB-PVD process. Both spray angle condition showed the formation and presence of

columnar grain structure which is visible as the single columnar grains. Due to the continuous deposition, the overlapping of columnar grain creates the misalignment which leads to formation

of pores and voids in the coating structure. The change in spray angle affects the grain growth behavior and distortion in the coating structure. The 90° spray angle samples shows closely packed dense columnar grain growth whereas the inclined 60° spray angle shows distributed columnar grains. In normal samples, the vertical growth of columnar grains were visible, whereas the inclined columnar grain growth behavior is observed in inclined spray angle. From surface microstructural study, it is found that the inclined spray angle leads to elongation in grain structure. This can be verified with cross-sectional structure which shows the inclination in columnar grains. The normal spray angle samples showed the large width columnar grain whereas the inclined showed the columnar grains with more length. The defects such as pores were more visible with more intra-columnar gaps in inclined than normal spray angle. The large of pores and voids can create the high shadow region leading to affect the coating roughness and hardness. Considering the top surface of columnar grain structure, the surface of normal samples were more uniform than inclined samples which showed the more variation in columnar heights. Therefore, the normal spray angle could result in better surface uniformity than inclined spray angle.

3.3 Porosity distribution

The presence of porous structure were measured based on defects like pores and crack produced during the deposition mechanism. The image analysis was performed to find the porous structure including cracks, surface irregularities and grain structures. Figure 8 and Figure 9 shows the SEM images used for porosity analysis and images generated using ImageJ by single channel RGB greyscale representing porosity and surface irregularities in black and coating in white. Out of all, E90 represents low amount of porosity as the coating is almost uniformly deposited with fine and dense grain structure. Whereas, the A60 showed the high porosity level due to the non-uniform surface and distributed grain structure. The A90 and E60 results in almost similar porosity level in the TBCs. The E90 results in low shadow region followed by E60 and A90 with further increase in shadow region for A60 condition. The low shadow region in the coating generated low amount of porosity and inverse leads to high porosity. The shape of the pores obtained in A60 results in more irregular shape compared to other samples.
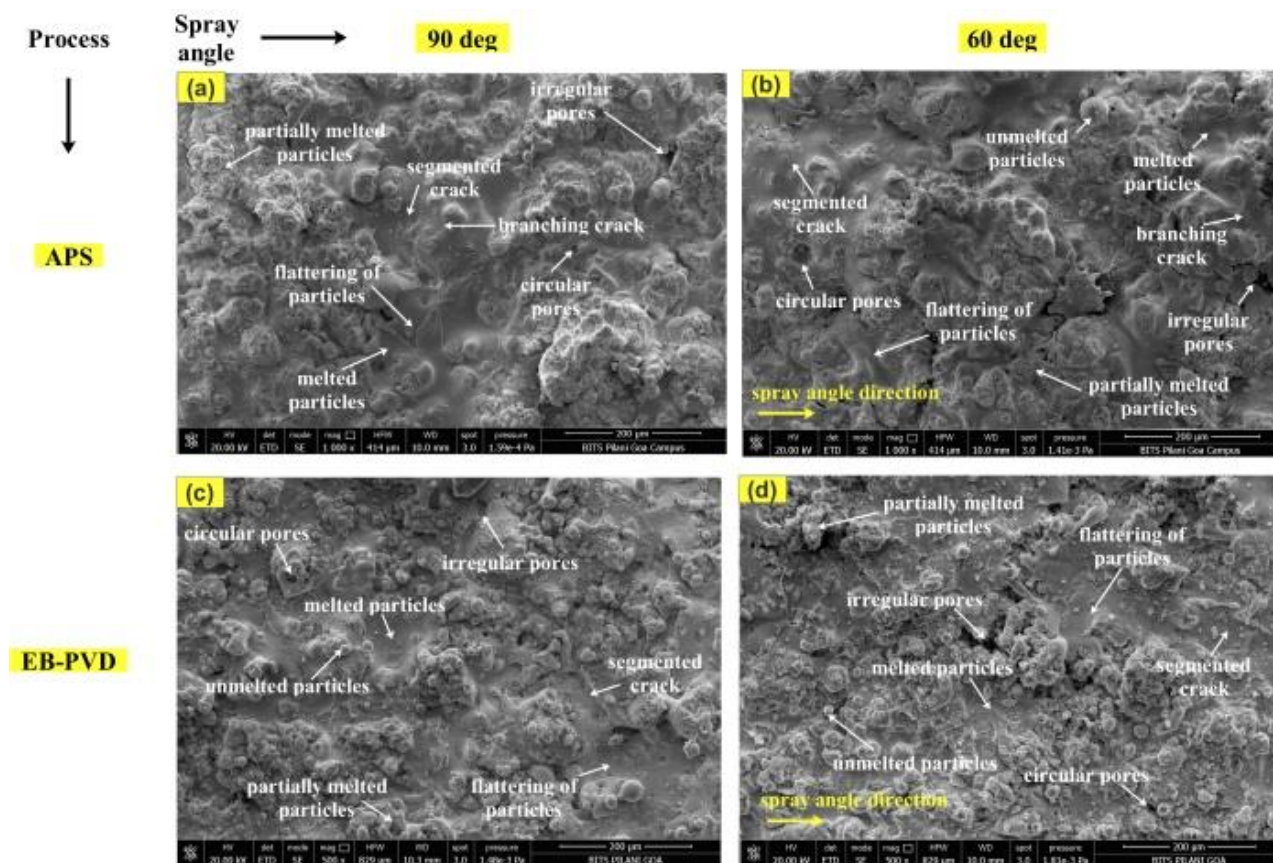

Fig. 8. SEM images used for porosity analysis of (a) APS 90°, (b) APS 60°, (c) EB-PVD 90°, and (d) EB-PVD 60° samples.
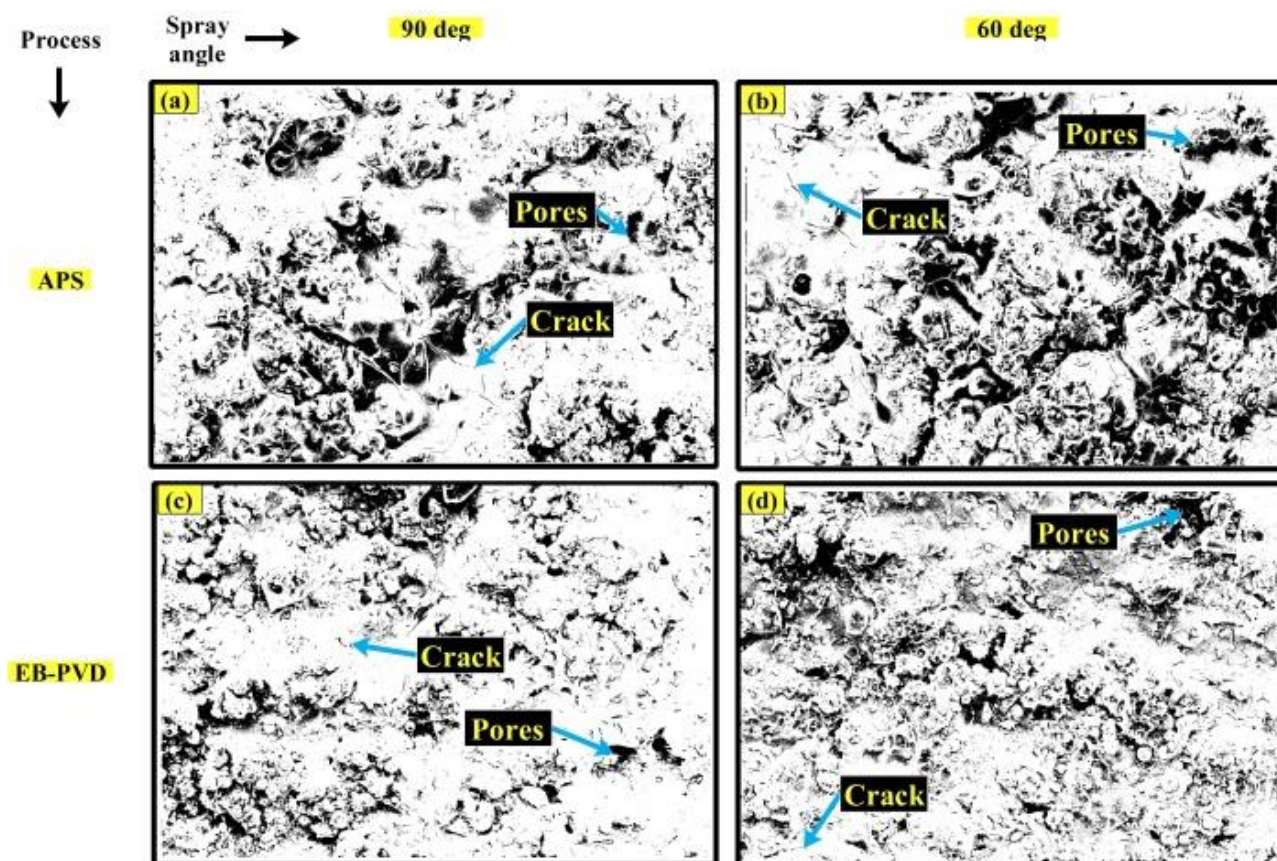
Fig. 9. Representation of porous structure showing in black and coating in white for (a) APS 90°, (b) APS 60°, (c) EB-PVD 90°, and (d) EB-PVD 60° samples.

Table 2 shows the porosity level in the APS and EB-PVD with change in spray angle. As the spray angle and process is changed, around 63.5% increase in the porosity level for A60 was observed compared to E90. Similarly, around 27.2% and 21% increase in the porosity level for E60 and A90 compared to E90. The spray angle leads to change in pores present in coating structure. The coating porosity is increased with decreased in the spray angle condition [27].

Table 2. Porosity level for APS and EB-PVD with spray angle.

Sample no.	Deposition process	Spray angle (°)	Porosity (%)	Avg. porosity (%)
A 90	APS	90	21.84	21.93
			21.39	
			22.56	
A 60	APS	60	29.53	29.63
			30.21	
			29.14	
E 90	EB-PVD	90	17.11	18.12
			19.26	
			17.98	
E 60	EB-PVD	60	22.78	23.05
			23.56	
			22.81	

3.4 Residual stress analysis

Figure 10 shows spectrum and band peak obtained for EB-PVD with 90°. The measurement of Raman spectra were in the range of 100 to 800 cm^{-1}. It also shows the Raman band peaks for tetragonal and monoclinic phase of 8YSZ at 147, 255, 315, 466, and 637 cm^{-1}. To find the residual stress generated, the Raman peak obtained near 640 cm^{-1} is used as it results to better ratio for signal-to-noise. The low porosity results in large residual stresses induced in the coating structure. For all the APS and EB-PVD enabled 8YSZ TBCs the compressive stresses were obtained. Table 3 represents the Raman modes, and avg. shift of peak with generation of residual stresses developed into the coating with APS and EB-PVD deposition mechanism and spray angle. From Table 3 it showed that the sample with low porosity results in high value of compressive residual stress than medium and high level of porosity. A similar study was conducted by Kadam [40,42], and they found that the high porous structure results in lower residual stresses than the low

porous structure. Also, Teixeira et al. [28] and Portinha [30] investigated the effect of porous on residual stresses and found that high porosity would lead to low residual stresses in the coating. Compared with the above work, it was found that the high porous structure also generates low residual stresses in the coating. To find the developed residual stresses, the Raman peak were recorded during the thermal loading and the shift difference were calculated which shows the linear relationship between applied stress and shift corresponding to 220MPa of residual stress for each cm^{-1} shift [28]. The avg. Raman shift for E90 i.e. with low porosity is 1.86 cm^{-1}, for the medium porosity i.e. A90 and E60 is 1.33 cm^{-1} and 1.53 cm^{-1} respectively, and for high level of porosity is 0.93 cm^{-1}.
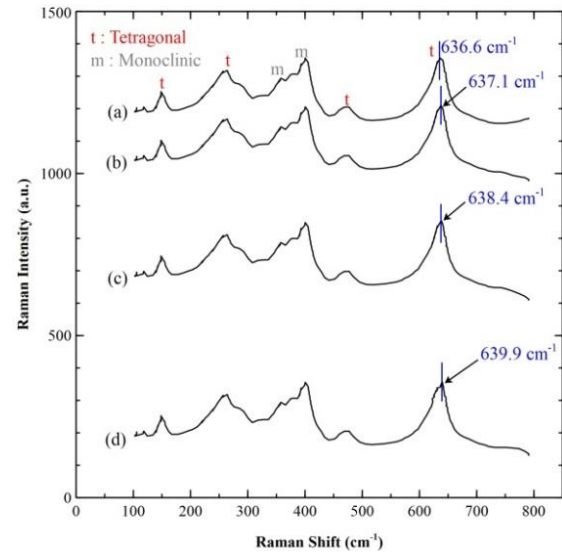

Fig. 10. Raman spectrum of sample E90 (a) EB-coated, (b) 5th, (c) 10th and (d) 15th cycle.

Table 3. Generation of residual stresses and its avg. shift.

Sample no.	Sample state	Raman modes (cm^{-1})	Difference (cm^{-1})	Avg. shift (cm^{-1})	Residual stress, σ (MPa)
A 90	as-coated	636.8	-	1.33	-
	5th	637.1	0.3		-66
	10th	638	1.2		-264
	15th	639.3	2.5		-550
A 60	as-coated	636.5	-	0.93	-
	5th	636.7	0.2		-44
	10th	637.4	0.9		-198
	15th	638.2	1.7		-374
E 90	EB-coated	636.6	-	1.86	-
	5th	637.1	0.5		-110
	10th	638.4	1.8		-396
	15th	639.9	3.3		-726
E 60	EB-coated	636.5	-	1.53	-
	5th	636.8	0.3		-66
	10th	638	1.5		-330
	15th	639.3	2.8		-616

3.5 Hardness analysis

Table 4 shows the hardness of APS and EB-PVD with change in spray angle. The E90 shows the high hardness value followed by A90, E60, and A60 condition. The E90 showed better surface in terms of uniformity, dense grain distribution resulting in low shadow region and porous contributing to high hardness. Whereas, as the spray angle is decreased, the defects are formed on large scale into the coating resulting decrease in hardness. Similar drop in hardness value was observed for APS deposition mechanism with spray angle change. From microstructural study, it was found that the high flattering of surface is generated due to better flow of molten particles, whereas low flattering was resulted due to

presence of partially melted particles. For 90°, around 6% and 7% increase in the hardness value was observed for E90 and A90 conditions for both APS and EB-PVD process compared with 60° condition. Similarly, around 2% change in the hardness was observed for E90 compared to A90, and 3% when compared with E60 to A60. Also, the hardness and roughness relationship with wear and friction was found, which showed the importance of coating over the substrate material [44-45]. It was observed that the higher value of coating hardness results in a lower wear rate. Based on the relationship, it was found that the 90° spray angle results in higher hardness and 60° results in lower hardness for APS and EB-PVD processes. Therefore, the APS and EB-PVD with a 90° spray angle would show a lower wear rate

than a 60° spray angle. Microstructural and hardness analysis found that changing the spray angle and using different deposition processes would change microstructural characterization [27, 40].

Table 4. Representation of hardness for APS and EB-PVD deposition mechanism with spray angle.

Sample no.	Deposition process	Spray angle (°)	Hardness (HV)	Avg. hardness (HV)
A 90	APS	90	825.2	842.6
			819.7	
			868.5	
			856.1	
			843.6	
A 60	APS	60	796.5	787.6
			783.2	
			785.9	
			791.4	
			780.9	
E 90	EB-PVD	90	849.7	858.2
			861.4	
			853.6	
			860.9	
			865.3	
E 60	EB-PVD	60	810.9	812.3
			805.6	
			815.4	
			811.1	
			818.5	

3.6 Roughness analysis

Table 5 represents roughness analysis for APS and EB-PVD deposition with spray angle. The surface roughness was obtained by traversing the profile across the surface at six different location and direction on each sample. The coating consists of molten particles with few unmelted, network of cracks, and presence of pores which can affect the roughness of the coating leading to non-uniform wear and irregular temperature drop across the structure. Also, the defects generate the rough surface leading to poor performance and early spallation in the coating. Therefore, to identify the uniformity over the surface, the roughness value is found. From Table 5, E90 showed the lowest value of the surface roughness amongst all, followed by E60, A90, and A60 condition. As E90 generates better surface uniformity leading to low porous structure resulting in smooth surface compared to other samples. Therefore, it can be seen that the APS results in rough surface generation compared to EB-PVD irrespective of change in spray angle. The

deposition rate for APS is high compared to EB-PVD which results in large presence of unmelted particles and defects leading to rough surface. Also, the surface's roughness contributes to the material's wear and friction properties. Even the smaller value of roughness leads to a smaller coefficient of friction, resulting in low wear of the coating material over the surface [45-48]. From microstructural and roughness analysis, it was found that the change in spray angle and deposition affects the coating properties. The similar study was conducted by Kadam et al. [27,40] and it was found that the change in spray angle would result in coating properties like roughness and hardness. Based on the relationship, it was found that the EB-PVD process showed better surface roughness, which would result in a low coefficient of friction, leading to a lower wear rate of the coating material over the substrate. Similarly, APS-coated samples would result in a high wear rate compared to EB-PVD due to the high value of surface roughness contributing to high friction. Compared with both deposition processes, the 90° spray angle would increase the lifespan of the coating as the surface roughness value is smaller than the 60° spray angle, which contributes to a lower coefficient of friction, resulting in a low wear rate.

Table 5. Representation of roughness for APS and EB-PVD deposition mechanism with spray angle.

Sample no.	Deposition process	Spray angle (°)	Ra (μm)	Avg. Ra (μm)
A 90	APS	90	9.516	9.327
			9.129	
			8.924	
			9.425	
			9.158	
			9.815	
A 60	APS	60	9.641	10.145
			10.812	
			10.597	
			9.973	
			10.157	
			9.691	
E 90	EB-PVD	90	8.874	8.792
			8.815	
			9.274	
			8.505	
			8.44	
			8.843	
E 60	EB-PVD	60	8.758	9.126
			9.129	
			9.637	
			8.969	
			9.416	
			9.118	

4. CONCLUSION

In this work, the APS and EB-PVD deposition mechanism for 8YSZ TBCs were studied and summarized from the microstructural and mechanical perspectives. Several conclusions were drawn from this study.

1. In APS, the primitives are formed in the shape of splat layer structure whereas the EB-PVD formed columnar structures.

2. The change in spray angle from 90° to 60° showed the inclined splat and columnar structure with elongation in grains.

3. The EB-PVD process result in fine grain structure with grain size in the range of 150 to 300nm, whereas APS showed in the range of 400 to 800nm.

4. The EB-PVD samples showed fine grains with densely distributed resulting in generation of low shadow region contributing to low amount of porosity compared to APS.

5. In EB-PVD deposition, the high amount of compressive residual stresses was generated when subjected to thermal loading compared to APS method. The avg. Raman shift for E90 i.e. low porosity - 1.86 cm^{-1}, medium porosity i.e. A90 and E60 is 1.33 cm^{-1} and 1.53 cm^{-1} respectively, and for high level porosity is 0.93 cm^{-1}.

6. For 90° spray angle, around 6% and 7% increase in the hardness value was observed for E90 and A90 for both APS and EB-PVD process compared with 60°. Similarly, around 2% change in the hardness was observed for E90 compared to A90, and 3% when compared with E60 to A60. The E90 showed the uniform surface roughness followed by E60, A90, and A60 samples.

Acknowledgement

REFERENCES

[1] R. Vaßen, M. O. Jarligo, T. Steinke, D. E. Mack, and D. Stöver, "Overview on advanced thermal barrier coatings," *Surface & Coatings Technology*, vol. 205, no. 4, pp. 938–942, Nov. 2010, doi: 10.1016/j.surfcoat.2010.08.151.

[2] T. S. Hille, T. J. Nijdam, A. S. J. Suiker, S. Turteltaub, and W. G. Sloof, "Damage growth triggered by interface irregularities in thermal barrier coatings," *Acta Materialia*, vol. 57, no. 9, pp. 2624–2630, May 2009, doi: 10.1016/j.actamat.2009.01.022.

[3] X. Cao, R. Vaßen, and D. Stoever, "Ceramic materials for thermal barrier coatings," *Journal of the European Ceramic Society*, vol. 24, no. 1, pp. 1–10, Jan. 2004, doi: 10.1016/s0955-2219(03)00129-8.

[4] D. Zhang, Z. Zhao, B. Wang, S. Li, and J. Zhang, "Investigation of a new type of composite ceramics for thermal barrier coatings," *Materials & Design*, vol. 112, pp. 27–33, Dec. 2016, doi: 10.1016/j.matdes.2016.09.050.

[5] A. M. Karlsson, "Modelling failures of thermal barrier coatings," *Key Engineering Materials*, vol. 333, pp. 155–166, Mar. 2007, doi: 10.4028/www.scientific.net/kem.333.155.

[6] L. Tang *et al.*, "Effects of spraying conditions on the microstructure and properties of NiCrBSi coatings prepared by internal rotating plasma spraying," *Surface & Coatings Technology*, vol. 374, pp. 625–633, Sep. 2019, doi: 10.1016/j.surfcoat.2019.06.056.

[7] D. Kumar and K. Pandey, "Optimization of the process parameters in generic thermal barrier coatings using the Taguchi method and grey relational analysis," *Proceedings of the Institution of Mechanical Engineers, Part L: Journal of Materials: Design and Applications*, vol. 231, no. 7, pp. 600–610, Aug. 2015, doi: 10.1177/1464420715602727.

[8] S. Mantry, R. K. Sahoo, B. B. Jha, B. K. Mishra, and M. Chakraborty, "Tribo-performance of plasma-sprayed nanostructured yttria-stabilized zirconia coatings using Taguchi's experimental design," *Proceedings of the Institution of Mechanical Engineers, Part J: Journal of Engineering Tribology*, vol. 228, no. 8, pp. 872–880, May 2014, doi: 10.1177/1350650114535385.

[9] J. G. Odhiambo, W. G. Li, Y. T. Zhao, and C. L. Li, "Porosity and its significance in Plasma-Sprayed coatings," *Coatings*, vol. 9, no. 7, p. 460, Jul. 2019, doi: 10.3390/coatings9070460.

[10] M. F. Morks, C. C. Berndt, Y. Durandet, M. Brandt, and J. Wang, "Microscopic observation of laser glazed yttria-stabilized zirconia coatings," *Applied Surface Science*, vol. 256, no. 21, pp. 6213–6218, Aug. 2010, doi: 10.1016/j.apsusc.2010.03.143.

[11] M. Izadinia, R. Soltani, and M. H. Sohi, "Formation of vertical cracks in air plasma sprayed YSZ coatings using unpyrolyzed powder," *Ceramics International*, vol. 46, no. 14, pp. 22383–22390, Oct. 2020, doi: 10.1016/j.ceramint.2020.05.320.

[12] J. Wang *et al.*, "Effect of spraying power on microstructure and property of nanostructured YSZ thermal barrier coatings," *Journal of Alloys and Compounds*, vol. 730, pp. 471–482, Jan. 2018, doi: 10.1016/j.jallcom.2017.09.323.

[13] J. Zhu and K. Ma, "Microstructural and mechanical properties of thermal barrier coating at 1400°C treatment," *Theoretical and Applied Mechanics Letters*, vol. 4, no. 2, p. 021008, Jan. 2014, doi: 10.1063/2.1402108.

[14] J. Ekberg, A. Ganvir, U. Klement, S. Creci, and L. Nordstierna, "The influence of heat treatments on the porosity of suspension Plasma-Sprayed Yttria-Stabilized zirconia coatings," *Journal of Thermal Spray Technology*, vol. 27, no. 3, pp. 391–401, Jan. 2018, doi: 10.1007/s11666-017-0682-y.

[15] U. Schulz, K. Fritscher and M. Peters, "EB-PVD Y_2O_3 and CeO_2/Y_2O_3 Stabilized Zirconia Thermal Barrier Coatings-Crystal Habit and Phase Composition," *Surface and Coatings Technolgogy*, vol. 82, pp. 259–69, 1996.

[16] U. Schulz, H. -j. Rätzer-Scheibe, B. Saruhan, and A. F. Renteria, "Thermal conductivity issues of EB-PVD thermal barrier coatings," *Materialwissenschaft Und Werkstofftechnik*, vol. 38, no. 9, pp. 659–666, Aug. 2007, doi: 10.1002/mawe.200700189.

[17] X. Zhang, J. Kulczyk-Malecka, J. Carr, P. Xiao, and P. J. Withers, "3D characterization of porosity in an air plasma-sprayed thermal barrier coating and its effect on thermal conductivity," *Journal of the American Ceramic Society*, vol. 101, no. 6, pp. 2482–2492, Jan. 2018, doi: 10.1111/jace.15409.

[18] A. Ganvir, N. Markocsan, and S. V. Joshi, "Influence of isothermal heat treatment on porosity and crystallite size in axial suspension plasma sprayed thermal barrier coatings for gas turbine applications," *Coatings*, vol. 7, no. 1, p. 4, Dec. 2016, doi: 10.3390/coatings7010004.

[19] T. Powell *et al.*, "Experimental investigation of the relationship between thermal barrier coating structured porosity and homogeneous charge compression ignition engine combustion," *International Journal of Engine Research*, vol. 22, no. 1, pp. 88–108, Jul. 2019, doi: 10.1177/1468087419843752.

[20] S. Cui *et al.*, "Mechanical analysis and modeling of porous thermal barrier coatings," *Applied Surface Science*, vol. 512, p. 145706, May 2020, doi: 10.1016/j.apsusc.2020.145706.

[21] B. K. Jang and H. Matsubara, "Influence of porosity on hardness and Young's modulus of nanoporous EB-PVD TBCs by nanoindentation," *Materials Letters*, vol. 59, no. 27, pp. 3462–3466, Nov. 2005, doi: 10.1016/j.matlet.2005.06.014.

[22] J. Krishnasamy, S. A. Ponnusami, S. Turteltaub, and S. Van Der Zwaag, "Computational investigation of porosity effects on fracture behavior of thermal barrier coatings," *Ceramics International*, vol. 45, no. 16, pp. 20518–20527, Nov. 2019, doi: 10.1016/j.ceramint.2019.07.031.

[23] L. Zhang *et al.*, "Velocity and temperature of In-Flight particles and its significance in determining the microstructure and mechanical properties of TBCs," *Acta Metallurgica Sinica (English Letters)*, vol. 32, no. 10, pp. 1269–1280, Mar. 2019, doi: 10.1007/s40195-019-00886-3.

[24] S.-W. Myoung, J. H. Kim, W.-R. Lee, Y. Jung, K.-S. Lee, and U. Paik, "Microstructure design and mechanical properties of thermal barrier coatings with layered top and bond coats," *Surface & Coatings Technology*, vol. 205, no. 5, pp. 1229–1235, Nov. 2010, doi: 10.1016/j.surfcoat.2010.08.063.

[25] M. Shi, X. Zhang, Z. Zhang, X. Ji, E. Byon, and S. Zhang, "Effect of spraying powder characteristics on mechanical and thermal shock properties of plasma-sprayed YSZ thermal barrier coating," *Surface & Coatings Technology*, vol. 395, p. 125913, Aug. 2020, doi: 10.1016/j.surfcoat.2020.125913.

[26] N. R. Kadam, G. Karthikeyan, and D. Kulkarni, "Effect of substrate rotation on the microstructure of 8YSZ thermal barrier coatings by EB-PVD," *Materials Today: Proceedings*, vol. 28, pp. 678–683, Jan. 2020, doi: 10.1016/j.matpr.2019.12.276.

[27] N. R. Kadam, G. Karthikeyan, and D. Kulkarni, "Effect of spray angle onto the microstructure of EB-PVD enabled 8YSZ thermal barrier coatings," *Materials Today: Proceedings*, vol. 44, pp. 1111–1117, Jan. 2021, doi: 10.1016/j.matpr.2020.11.187.

[28] V. Teixeira, M. Andritschky, W. Fischer, H. P. Buchkremer, and D. Stöver, "Analysis of residual stresses in thermal barrier coatings," *Journal of Materials Processing Technology*, vol. 92–93, pp. 209–216, Aug. 1999, doi: 10.1016/s0924-0136(99)00157-0.

[29] A. Scrivani *et al.*, "Thermal fatigue behavior of thick and porous thermal barrier coatings systems," *Journal of Thermal Spray Technology*, vol. 16, no. 5–6, pp. 816–821, Oct. 2007, doi: 10.1007/s11666-007-9128-2.

[30] A. Portinha *et al.*, "Residual stresses and elastic modulus of thermal barrier coatings graded in porosity," *Surface & Coatings Technology*, vol. 188–189, pp. 120–128, Nov. 2004, doi: 10.1016/j.surfcoat.2004.08.014.

[31] D. Kumar, K. Pandey, and D. K. Das, "Characterization of air plasma based 7YSZ aluminum alloys thermal barrier systems for hot zone," *Proceedings of the Institution of Mechanical Engineers, Part L: Journal of Materials: Design and Applications*, vol. 232, no. 7, pp. 582–591, Mar. 2016, doi: 10.1177/1464420716640570.

[32] "Introduction to coating design and processing," in *ASM International eBooks*, 2013, pp. 76–88. doi: 10.31399/asm.hb.v05a.a0005725.

[33] G. Montavon, S. Sampath, C. C. Berndt, H. Herman, and C. Coddet, "Effects of the spray angle on splat morphology during thermal spraying," *Surface & Coatings Technology*, vol. 91, no. 1–2, pp. 107–115, May 1997, doi: 10.1016/s0257-8972(96)03137-4.

[34] J. Ilavský, A. J. Allen, G. G. Long, S. Krueger, C. C. Berndt, and H. Herman, "Influence of spray angle on the pore and crack microstructure of Plasma-Sprayed deposits," *Journal of the American Ceramic Society*, vol. 80, no. 3, pp. 733–742, Mar. 1997, doi: 10.1111/j.1151-2916.1997.tb02890.x.

[35] Nikhil Kadam, G. Karthikeyan Dhananjay Kulkarni, "The effect of spray angle on the microstructural and mechanical properties of plasma sprayed 8YSZ TBCs, " *in 11th International Conference on Precision, Meso, Micro and Nano Engineering (COPEN 2019)*, 2019.

[36] H. Du, S. W. Lee, and J. H. Shin, "Study on Porosity of Plasma-Sprayed Coatings by Digital Image Analysis Method," *Journal of Thermal Spray Technology*, vol. 14, no. 4, pp. 453–461, Dec. 2005, doi: 10.1361/105996305x76450.

[37] N. Curry, M. Leitner, and K. Körner, "High-Porosity Thermal Barrier Coatings from High-Power Plasma Spray Equipment—Processing, Performance and Economics," *Coatings*, vol. 10, no. 10, p. 957, Oct. 2020, doi: 10.3390/coatings10100957.

[38] W. Tillmann, O. Khalil, and M. Abdulgader, "Porosity characterization and its effect on thermal properties of APS-Sprayed alumina coatings," *Coatings*, vol. 9, no. 10, p. 601, Sep. 2019, doi: 10.3390/coatings9100601.

[39] E. Garcia, P. Miranzo, R. Soltani, and T. W. Coyle, "Microstructure and thermal behavior of thermal barrier coatings," *Journal of Thermal Spray Technology*, vol. 17, no. 4, pp. 478–485, Oct. 2008, doi: 10.1007/s11666-008-9200-6.

[40] N. R. Kadam, G. Karthikeyan, and D. Kulkarni, "The effect of spray angle on the microstructural and mechanical properties of plasma sprayed8YSZ thermal barrier coatings," *Journal of Micromanufacturing*, vol. 5, no. 2, pp. 181–192, Jun. 2021, doi: 10.1177/25165984211016323.

[41] N. Kadama, G. Karthikeyan, D. Kulkarni, and P. Jagtap, "Microstructural characterization, residual stress, and mechanical properties of plasma sprayed 8YSZ thermal barrier coatings," *Tribology in Industry*, vol. 44, no. 1, pp. 230–243, Jun. 2022, doi: 10.24874/ti.1105.05.21.07.

[42] P. Kadam, N. Kadam, G. Karthikeyan, D. M. Kulkarni, A. Damale, "Microstructural, Thermo-physical and Mechanical Characterization of a Laser Remelted Plasma Sprayed NiCrAlY/8YSZ Thermal Barrier Coating (TBC) on Inconel 718," *Lasers In Engineering*, vol. 55, no. 1-2, pp. 3-19, 2023.

[43] Nikhil R. Kadam, "Investigation of Double Top Layer Coating with APS and EB-PVD for High Temperature Surfaces", PhD dissertation, BITS Pilani, India, 2022.

[44] K. H. Zum Gahr, "Microstructure and wear of materials," *Tribology Series*, vol. 10, pp. 174-176, 1987.

[45] K. Kato, "Wear in relation to friction — a review," *Wear*, vol. 241, no. 2, pp. 151–157, Jul. 2000, doi: 10.1016/s0043-1648(00)00382-3.

[46] O. Sagalovicha, V. Popov, V. Sagalovich, S. Dudnik, and O. Olijnyk, "Working out the processes of deposition "MetalMetal" Multi-Layer coatings (CU-MO, CU-MON, CU-C) and studying the tribological characteristics of friction pairs," *Journal of Materials and Engineering*, vol. 1, no. 1, pp. 26–37, Jan. 2023, doi: 10.61552/jme.2023.01.004.

[47] H. Kim, K. Kato, "Lubrication properties of tribo-coating in ultra high vacuum," *Proc. Euro-Trib'93*, 1993.

[48] N. R. Kadam, G. Karthikeyan, P. M. Jagtap, and D. Kulkarni, "An atmospheric plasma spray and electron beam-physical vapour deposition for thermal barrier coatings: a review," *Australian Journal of Mechanical Engineering*, vol. 21, no. 5, pp. 1729–1754, Jan. 2022, doi: 10.1080/14484846.2022.2030088.